Numerical Simulation of Potential Step Chronoamperometry at Low Concentrations of Supporting Electrolyte

Ian Streeter and Richard G. Compton*

Department of Chemistry, Physical and Theoretical Chemistry Laboratory, Oxford University, South Parks Road, Oxford, United Kingdom OX1 3QZ

Received: May 20, 2008; Revised Manuscript Received: June 20, 2008

Electrochemical systems are considered for which the concentration of ions in solution is low, and therefore there is an electric field which extends deep into solution away from the electrode surface. Finite difference methods are used to model a potential step chronoamperometry experiment at a microhemisphere electrode. Concentration profiles, potential profiles, and current−time curves are presented for a range of electrochemical systems and physical parameters. The model uses the Nernst−Planck−Poisson system of equations to model mass transport and includes a description of the electrical double layer at the working electrode surface. Two approximations are then considered as a means of greatly simplifying the model while retaining accuracy under certain conditions. These are the approximation of a negligibly small electrical double layer and the approximation of electroneutrality. It is concluded that the former approximation is both more appropriate than the latter approximation and more conveniently implemented in terms of CPU simulation times.

Introduction

For electrochemical experiments in which a current is driven at an electrode, it is common to have an inert supporting electrolytic salt dissolved in solution. Its purpose is to distort the electric field that exists at the electrode−solution interface in a region known as the electrical double layer (EDL). The charged species provided by the inert salt can separate near the electrode surface in such a way that the EDL becomes narrower and the electric field stronger. The narrowing of the electric field with added supporting electrolyte is favorable for driving a heterogeneous electron transfer and for making electrochemical measurements. When a faradaic process is driven, charge is passed across the electrode−solution interface. The supporting electrolyte is able to retain the favorable electric field profile during this process, by migrating to negate the excess charge created at the electrodes. This process is often described as the electrolyte improving the conductivity of the solution, therefore reducing the ohmic potential drop.

The mass transport of the electroactive species through a fully supported solution is entirely due to diffusion, except in the EDL where migration may be important. The kinetics of a heterogeneous electron transfer are typically dependent on the potential difference across the electrode−solution interface. When the electric field is confined to such a narrow region, this potential difference is approximately equal to that between the working electrode and the bulk solution. A supported electochemical experiment can therefore be described by a relatively simple model in which mass transport is by diffusion only, and there are simple rate equations for the processes at the electrode surface. For example, potential step chronoamperometry at a planar macroelectrode can be described by the Cottrell equation, which is based on theory dating back to 1903.[1]

Unfortunately, the use of supporting electrolyte can introduce other problems to an experiment. For example, measurements can be distorted by complexation of the supporting electrolyte to the species of interest, the increased ionic strength can alter the thermodynamic and kinetic properties of the system, and there is an increased risk of contamination by impurities. Furthermore, many nonpolar solvents are not even capable of dissolving large amounts of electrolyte salts. Progress was made in negating these problems when it was found that supporting electrolyte was not necessary to drive a faradaic current at a microelectrode.[2−4] Such little current is drawn at such a small electrode that the ohmic potential drop across the cell is small, and the current can be carried in solution by relatively low concentrations of charged species.

A more complex model is needed to interpret experimental currents recorded in weakly supported media, to account for the electric field which extends deep into solution away from the electrode. Diffusion and migration can both contribute to the mass transport of the electroactive species, and the electrode kinetics suffer from Frumkin effects[5] since the potential driving force across the electrode−solution interface is no longer equal to the potential difference between the bulk phases

In this work, we model chronoamperometry in weakly supported media using the Nernst−Planck−Poisson (NPP) system of equations. The NPP equations are based on the Nernst−Planck expression for the diffusion−migration of a charged species in an electric field, and the Poisson equation for the electric field as a function of charge. These equations are described in more detail in subsection 2.2. The NPP equations have been successfully applied by other researchers to model faradaic processes under conditions where the potential drop through solution is important.[6−13] In particular, Norton et al. calculated the mass transport limiting currents at a hemispherical electrode and showed that significant deviations from classical behavior are predicted when the electrode is small compared to the electrical double layer.[7] Smith and White,[9] He et al.,[12] and Yang and Zhang[13] all extended this work by calculating the steady-state currents at electrodes of nanometer dimensions, but each using a slightly different model for the electrical double layer. The approach established by these workers is to model each species in solution simultaneously,

* Corresponding author. Fax: +44 (0) 1865 275410. Tel: +44 (0) 1865 275413. Email: richard.compton@chem.ox.ac.uk.

10.1021/jp804442m CCC: $40.75
Published on Web 08/13/2008

including inert anions and cations, and allowing a diffuse electrical double layer to form at the electrode by the separation of charged species. The boundary conditions used at the electrode surface account for the kinetic effect that the potential drop through solution has on the electron transfer. Our simulation approach and model of the EDL is similar to that of He et al. except that we calculate the transient current response.

Other researchers have tackled the problem of modeling diffusion−migration systems by applying the approximation of electroneutrality. This idea was originally proposed by Planck to model the concentration and potential profiles at a liquid junction.[14−16] The approximation follows from the observation that there is often very little separation of positive and negative ions in a depletion layer. This is an attractive approximation to apply to faradaic processes, since it means that the diffuse double layer need not be modeled. However, the assumption can be inadequate for low concentrations of electrolyte,[17] and cannot be justified if the diffuse double layer is comparable in size to the depletion layer.[7] The current measured at a microhemisphere electrode has been modeled using the electroneutrality approximation for steady state[18−22]and transient conditions.[23−26]

The current−time behavior for a potential step experiment at a microelectrode has only ever been modeled using the electroneutrality approximation; researchers who avoided this approximation only calculated the steady-state limiting current. In this work, we solve the NPP equations using finite difference methods to generate current−time curves for a potential step, while avoiding the approximation of electroneutrality. We note that the NPP equations have been solved previously for the time evolution of various transient systems, although not for this particular faradaic process. For example, the time evolution of liquid junctions[27−33] and the injection of charge into an ideally polarizable electrode[33−35] have both been tackled.

Section 2 describes in further detail the model that we use to describe the potential step experiment, and the simulated concentration and potential profiles and current−time curves are presented in section 3. In section 4 we make some simplifying approximations to the theoretical model, including the approximation of electroneutrality, and compare the new current−time current curves with those of the original model

2. Theoretical Model

2.1. Systems under Consideration. A number of different species feature in solution in this model of a potential step chronoamperometry experiment. These species are denoted A^z, B^{z+1}, M^+, and X^-. The species M^+ and X^- are electrochemically inert, and are used as supporting electrolyte. Species A^z is the electroactive species, and species B^{z+1} is the electrogenerated product, where z represents the ionic charge.

$$A^z - e^- \rightleftarrows B^{z+1} \quad (1)$$

In this work, we consider an electroactive species which is either neutral ($z_A = 0$)or a singularly charged anion ($z_A = -1$)The bulk solution concentration of the electroactive species is written C^*, and the concentration of additionally added supporting electrolyte is written C_{sup}. When species A is charged, it is accompanied in bulk solution by an equivalent amount of the neutral cation M^+; the bulk concentration of species M^+ is therefore equal to $C^* + C_{sup}$ if $z_A = -1$

The electrode configuration under consideration is shown in Figure 1. We choose to model a hemispherical working electrode, because the mass transport equations for this geometry form a one-dimensional problem. A reference electrode of arbitrary shape is placed sufficiently far from the working

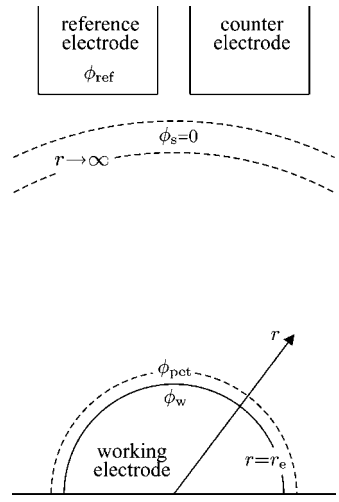

Figure 1. Electrode configuration and important values of the potential, ϕ.

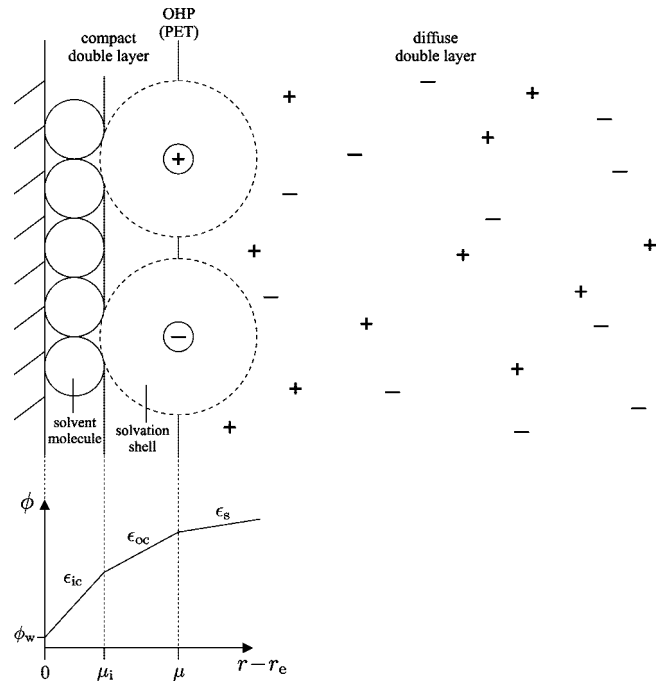

Figure 2. Schematic diagram of the electrical double layer at the electrode as modeled in our simulations. The parameters ϵ_{ic}, ϵ_{oc}, and ϵ_s are the dielectric constants in the different regions of the EDL.

electrode that we may consider the electric potential to tend toward a constant value as r tends toward infinity. The working electrode has radius r_e, and the values ϕ_w, ϕ_s, and ϕ_{ref} refer to the absolute potentials of the working electrode, bulk solution, and the reference electrode, respectively. A counter electrode is also present, as is typical for an experimental electrochemical cell. It is assumed to be sufficiently far from the other two electrodes that it does not interfere with the concentration or potential profiles

Figure 2 shows the model used for the interface between the working electrode and the solution. This is the model that was successfully used by He et al. to simulate the mass transport limiting steady-state current for similar electrochemical systems.[12] The electrical double layer is analogous to the Stern model for the equilbrium EDL at zero current: it consists of a compact part of thickness μ, and a diffuse part, which extends deeper into solution. The boundary between these two regions is the outer Helmholtz plane (OHP), which is found at $r = r_e$

$+ \mu$. The OHP represents the plane of closest approach for each chemical species in solution; there is no specific adsorption on the electrode surface, and therefore the compact region is always uncharged. In the diffuse part of the EDL and in the solution beyond the EDL, the species are treated as point charges and are described by their mean local concentrations. Unlike the compact EDL, the diffuse region can have an overall nonzero charge; this corresponds to differences in the mean local concentrations of the various charged species

The dielectric properties of a solution become distorted in the region near an electrode interface, and the effective dielectric constant varies continuously with r across the EDL. The model shown in Figure 2 approximates this behavior by using two different values of the dielectric constant in the compact part of the double layer. The value ϵ_{ic} is for the inner part of the compact EDL, which has a thickness μ_i and refers to the first layer of solvent molecules adsorbed on the electrode surface. The value ϵ_{oc} is for the outer part of the compact EDL, and refers to the uncharged solvation shell surrounding the species situated on the OHP. The bulk solution dielectric constant, ϵ_s, is used for the diffuse EDL and beyond

The potential in solution varies from its value ϕ_s in bulk solution to the value ϕ_w at the surface of the working electrode. The oxidation of species A occurs at its closest approach to the electrode surface, which is the OHP. This plane is therefore also referred to as the plane of electron transfer (PET). The electron transfer is driven by the potential difference across the electrode−solution interface, $\phi_w - \phi_{pet}$, where ϕ_{pet} is the potential in solution at the PET, as shown in Figure 1.

The cell potential is denoted E, which is equal to $\phi_w - \phi_{ref}$, and the corresponding formal cell potential is $E_f^{\ominus}$. The reference electrode is assumed to have ideal behavior; therefore, a change to the cell potential is manifested as a change to the potential difference between the working electrode and the bulk solution. It is often stated in electrochemical literature that it is not possible to directly measure this "half-cell" potential difference between the working electrode and bulk solution. In this work, we set this classically unmeasurable potential difference by referring to the cell potential of zero charge, E_{pzc}, which it is possible to measure, for example by electrocapillary experiments. In a model that does not account for potential drop due to the orientation of solvent molecules, the value E_{pzc} corresponds to the potential applied to the cell such that there is a zero potential difference between the working electrode and the solution. The potential of zero charge has appeared as an important parameter in previous simulations of the faradaic current at a microelectrode, but it was generally set equal to the formal electrode potential.[9]

The electrochemical experiment that we simulate consists of two steps and represents a typical potential step experiment. Initially, the working electrode is held at a reducing potential and the system is allowed to reach a state of equilibrium such that no current flows, but a diffuse double layer is established at the electrode−solution interface. The electrode potential is then instantaneously stepped to a more positive potential, such that species A is oxidized and a faradaic current is driven. Furthermore, the EDL is perturbed by this change in electrode potential, and there is therefore an additional nonfaradaic contribution to the current due to the charging of the working electrode surface. In this work, we calculate each contribution to the current as a function of time

2.2. Nernst−Planck−Poisson Equations. The mass transport of each species i in solution is described by the Nernst−Planck expression

$$\mathbf{J}_i = -D_i\left(\nabla C_i + z_i C_i \frac{F}{RT}\nabla \phi\right) \tag{2}$$

where $\mathbf{J}_i$ is a vector representing the flux of the species, D_i is a diffusion coefficient, C_i is the concentration, z_i is the species charge, and all other terms have their usual meanings. The first right-hand term in eq 2 describes the diffusion of the species along a concentration gradient, and the second term describes the migration of a charged species in an electric field. The evolution of the concentration profile with time is found by solving the continuity equation for the conservation of mass

$$\frac{\partial C_i}{\partial t} = -\nabla \cdot \mathbf{J}_i \tag{3}$$

At all times, the electric field in solution must satisfy the Poisson equation:

$$\nabla^2 \phi = -\frac{\rho}{\epsilon_r \epsilon_0} \tag{4}$$

where ρ is the local charge density, ϵ_r is the dielectric constant of the medium, and ϵ_0 is the permittivity of space. The charge density can be expressed in terms of the local concentrations of the charged species in solution

$$\rho = F\sum_i z_i C_i \tag{5}$$

The concentration profiles of the various species and the potential profile throughout solution can be found by using numerical methods to simultaneously solve eqs 3 and 4 for each species. This system of equations is collectively known as the Nernst−Planck−Poisson (NPP) equations. The NPP equations for a hemispherical electrode are one-dimensional; they are a function of only the spherical radial coordinate, r. The set of equations to be solved are written here in terms of the transformed coordinate, y

$$y = 1 - \frac{r_e}{r} \tag{6}$$

where r_e is the radius of the electrode. The coordinate y scales between the values 0 and 1, corresponding to the electrode surface and an infinite distance from the electrode, respectively. However, we solve the NPP equations between the limits $\mu' \leq y \leq 1$, where μ' is the value of y corresponding to the PET. Before we solve the NPP equations, we normalize them by expressing them in terms of dimensionless parameters. Dimensionless time, τ, is given by

$$\tau = \frac{F^2 D C^* t}{RT\epsilon_s \epsilon_0} \tag{7}$$

where C^* is the bulk concentration of the electroactive species. The concentration of each species is expressed as a fraction of this bulk concentration

$$c_i = \frac{C_i}{C^*} \tag{8}$$

Dimensionless potentials, θ, are given by

$$\theta = \frac{F\phi}{RT} \tag{9}$$

Using this dimensionless system, eq 3 becomes

$$\frac{\partial c_i}{\partial \tau} = \frac{(1-y)^4}{{R_e}^2}\left(\frac{\partial^2 c_i}{\partial y^2} + z_i c_i \frac{\partial^2 \theta}{\partial y^2} + z_i \frac{\partial c_i}{\partial y}\frac{\partial \theta}{\partial y}\right) \quad (10)$$

and the Poisson equation becomes

$$\frac{(1-y)^4}{{R_e}^2}\frac{\partial^2 \theta}{\partial y^2} = -\sum_i z_i c_i \quad (11)$$

Equations 10 and 11 contain a parameter R_e, which can be thought of as the dimensionless electrode radius

$$R_e = r_e\left(\frac{F^2 C^*}{RT\epsilon_s\epsilon_0}\right)^{1/2} \quad (12)$$

We have made the assumption here that the diffusion coefficients of all species are equal, but note that when modeling a real system it will not be complicated to include different diffusion coefficients

Equations 10 and 11 are solved subject to appropriate boundary conditions, which are summarized in Table 1 and discussed here in more detail. The boundary conditions at $y = 1$ describe the concentrations and the potential in bulk solution. The potential in bulk solution is set as $\phi_s = 0$, and all other potentials are set relative to this value.

The boundary conditions at $y = \mu'$ describe the flux of each species at the PET in terms of the dimensionless flux density, J_i

$$J_i = -\left(\frac{\partial c_i}{\partial y} + z_i c_i \frac{\partial \theta}{\partial y}\right) \quad (13)$$

The boundary condition for the electroactive species is given by Butler−Volmer kinetics

$$J_A = -K_0 \exp((1-\alpha)\Delta\theta)c_A + K_0 \exp(-\alpha\Delta\theta)c_B \quad (14)$$

where the value $\Delta\theta$ describes the potential driving force between the electrode and the plane of electron transfer

$$\Delta\theta = \frac{F}{RT}\Delta\phi = \frac{F}{RT}(E - E_f^{\ominus}) - \theta_{pet} \quad (15)$$

Large currents are driven at the electrode when the value $\Delta\theta$ is large and positive. Equation 14 uses a charge transfer coefficient, α, and a dimensionless rate constant, K_0, defined in eq 16 where k_0 is the dimensional standard heterogeneous rate constant

$$K_0 = \frac{k_0 r_e}{D} \quad (16)$$

The boundary condition for the potential at the PET is found by consideration of the potential of the electrode surface, θ_w, and the electric field within the compact double layer

$$\theta_{pet} = \frac{F}{RT}(E - E_{pzc}) + \frac{r_e}{r_e + \mu_i}\left(\frac{\mu_i \epsilon_s}{r_e \epsilon_{ic}} + \frac{(\mu - \mu_i)\epsilon_s}{(r_e + \mu)\epsilon_{oc}}\right)\frac{\partial \theta}{\partial y} \quad (17)$$

Equation 17 is similar to the boundary condition used by He et al. in their equivalent model of unsupported electrolysis.[12] It is derived by applying the Poisson equation to describe the potential gradient across the electrically neutral compact double layer. This derivation is presented in Appendix 1. Note that it is in implementing boundary condition (17) that the cell potential of zero charge becomes an important parameter in this model.

Further boundary conditions are required to describe the initial conditions of the system at $t = 0$, the time of the potential step. This corresponds to the system in a state of equilibrium when the working electrode is held at a reducing potential such that no current flows. We use the term "equilibrium" diffuse double layer to describe the structure of the EDL at $t = 0$. The concentration of ions in an equilibrium double layer are described by the Boltzmann distribution

$$c_i = c_i^b \exp(-z_i\theta) \quad (18)$$

where c_i^b is the bulk dimensionless concentration. The potential throughout solution is described by eq 11, which is combined with eq 18 to give the Poisson−Boltzmann equation

$$\frac{(1-y)^4}{{R_e}^2}\frac{\partial^2 \theta}{\partial y^2} = -\sum_i z_i c_i^b \exp(-z_i\theta) \quad (19)$$

The potential profile is calculated by numerically solving eq 19 subject to boundary condition (17). The equilibrium concentration of each species is then found by applying eq 18. Note that the Boltzmann distribution is not used at times $t > 0$, for which equilibrium relationships are not appropriate.

The partial differential equations describing the theoretical model are discretized using finite difference methods and solved using the iterative Newton−Raphson method. Appendix 2 gives further details on the methods used to solve these equations. The equations are discretized nonlinearly along the y coordinate such that the highest density of nodes is found at the electrode surface where the EDL effects steep concentration gradients. The magnitude of the discretized time increment, $\Delta\tau$, also increases as the simulation progresses for greater efficiency. The simulation program has been tested for convergence by ensuring that an increase in the number of spatial or temporal nodes leads to a negligible change in the simulated current.

2.3. Calculating the Current. In subsection 2.1 it was stated that there are both faradaic and nonfaradaic contributions to the current. Equation 20 shows the equation used to calculate the current at the hemispherical electrode, where the derivatives with respect to y are taken as the concentration gradient and potential gradient in the diffuse EDL at the PET

$$\frac{i}{i_{lim}} = \left(\frac{\partial c_A}{\partial y} + z_A c_A \frac{\partial \theta}{\partial y}\right) + \frac{\partial}{\partial \tau}\frac{\partial \theta}{\partial y} \quad (20)$$

The value i_{lim} in eq 20 is the mass transport limiting current assuming a diffusion-only model; this is the steady-state current expected in a fully supported electrolyte when an extreme potential is applied to the working electrode. The value of i_{lim} is known as an analytical expression

$$i_{lim} = 2\pi F D C^* r_e \quad (21)$$

The terms in parentheses in eq 20 are equal to the dimensionless flux of species A through the electrode surface and represent the faradaic contribution to the current. The last term in eq 20 is for the nonfaradaic contribution. This is proportional to the rate of change of the charge on the electrode, which in turn is proportional to the rate of change of the electric field near the electrode surface

TABLE 1: Boundary Conditions for the NPP Equations

species/potential	$y = \mu'$	$y = 1$
A	Butler−Volmer	$c_A = 1$
B	$J_A = J_B$	$c_B = 0$
M^+	$J_{M^+} = 0$	$c_{M^+} = \lvert z_A\rvert^+ c_{sup}$
X^-	$J_{X^-} = 0$	$c_{X^-} = c_{sup}$
θ	eq *17*	$\theta = 0$

3. Simulated Results

3.1. Physical Parameters. The electrochemical system and experiment that we have chosen to simulate is characterized by a large number of physical parameters. We do not attempt to demonstrate the effect that each parameter has on the simulated current−time behavior. Rather, we choose typical parameters for an electrochemical experiment in aqueous media and demonstrate some of the more interesting effects that are observed with changing the physical parameters.

The electroactive species is present at a concentration of 1 mM. When the electroactive species is charged, we consider the experiment with no additional supporting electrolyte, and when it is neutral we use a supporting electrolyte concentration of 0.1 mM. We also consider the experiments with a supporting electrolyte concentration of 100 mM, noting that this is typical for a "fully supported" classical electrochemistry experiment. Each species has a diffusion coefficient of $D = 10^{-5}$ cm^2 s^{-1}.

The radius of the electrode is either 100 nm or 10 μm. Smaller electrodes are expected to give greater deviations from the diffusion-only model behavior. However, with a radius smaller than 100 nm, the transient part of the current−time plot occurs at extremely short times, and the experimentally observable current is essentially the steady-state current. The steady-state NPP equations solved by He et al.[12] or Yang and Zhang[13] are more appropriate for such systems

The electron transfer has a fast rate constant of $k_0 = 1$ cm s^{-1}, and a typical charge transfer coefficient of $\alpha = 0.5$. The temperature is 298 K, at which the relative dielectric constant of water is $\epsilon_s = 80$ in bulk solution. The size of the compact layer is described by the parameters $\mu = 0.6$ nm and $\mu_i = 0.29$ nm, which are approximate values that come from considering the hard-sphere diameter of a water molecule.[36] The relative dielectric constants for the inner and outer parts of the compact layer are $\epsilon_{ic} = 6$ and $\epsilon_{oc} = 40$, which come from a consideration of the orientation of the water molecule dipoles in this region.[36]

The formal electrode potential for the A/B couple is set to be $E_f^{\ominus} = 0$ V. For the initial conditions of the experiment, the cell potential is held at −0.25 V so that no current flows. At $t = 0$, the cell potential is instantaneously stepped to +0.25 V. This potential is sufficiently oxidizing that a diffusion-only model would predict the current to tend toward the mass transport limiting value, i_{lim}, from eq 21.

3.2. Simulated Concentration Profiles. Over the course of the simulated chronoamperometry experiment, the potential applied to the working electrode effects some interesting changes to the concentration profiles and potential profiles through solution. In this section, some of these interesting features of the modeled system are highlighted and used to explain the observed current response

Figure 3 shows some concentration and potential profiles, corresponding to immediately before and immediately after the potential step. The profiles are for a 10 μm radius hemisphere when species A is charged ($z_A = -1$), there is no additional supporting electrolyte, and the cell potential of zero of charge is $E_{pzc} = 0$ V. Immediately before the potential step, the cell potential is at −0.25 V with respect to the formal potential and there is a positively charged diffuse double layer consisting of an excess of M^+ and a depletion of A^- ions. The majority of the electric field is confined to within 0.04 μm of the electrode surface, and there is no potential gradient through the rest of the solution. Immediately after the potential step the cell potential is +0.25 V with respect to the formal potential. The diffuse double layer cannot respond immediately to this change in potential,

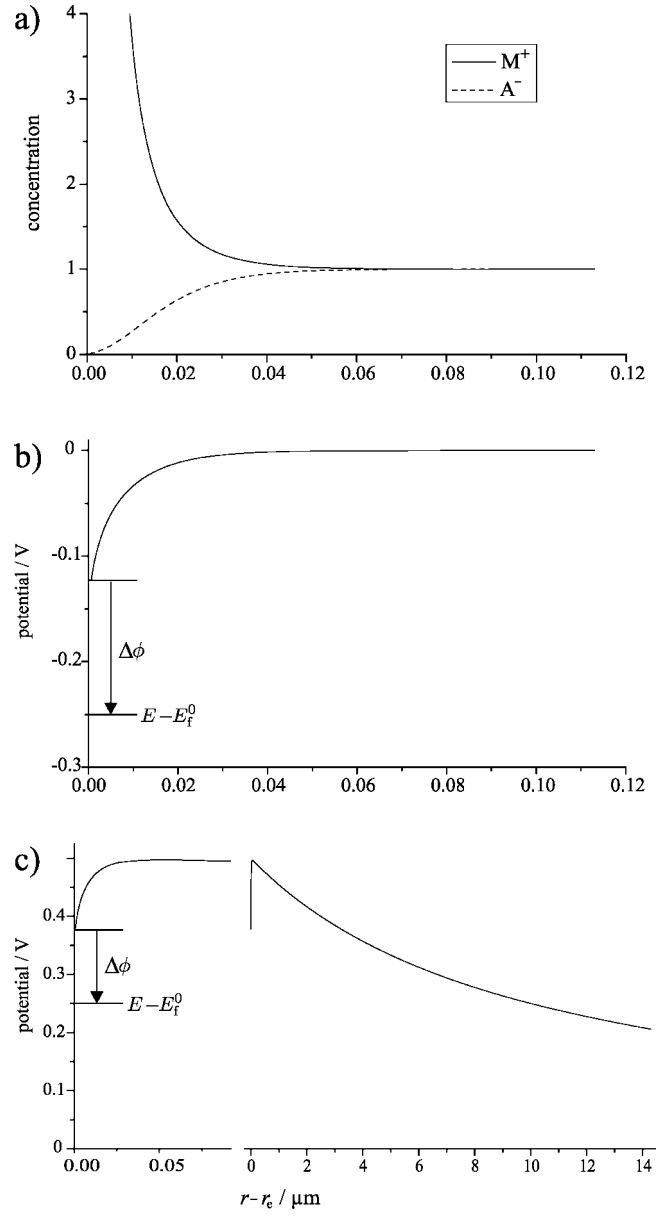

Figure 3. Profiles of (a) the dimensionless concentration and (b, c) the potential through solution at a 10 μm hemisphere: (a) and (b) are immediately before and (c) is immediately after the potential step. The electroactive species is charged ($z_A = -1$), there is no additional supporting electrolyte, and $E_{pzc} = 0$ V. The region near the electrode is shown again in part c in closer detail.

and so the form of the electric field within 0.04 μm of the electrode surface is unchanged. However, there is now a potential gradient that extends beyond the double layer and only approaches zero as $r \rightarrow \infty$. The potential profiles show the value $\Delta\phi$, which was introduced in eq 14 as the potential driving force for the electron transfer. Immediately after the electron transfer the value of $\Delta\phi$ is negative, so there is very little potential driving force for the electron transfer.

Figure 4 shows concentration and potential profiles for the same system at 0.01 s after the potential step. Mass transport of the charged species has led to a diffuse EDL which is now negatively charged, consisting of an excess of A^- and a depletion of M^+ ions. The change in charge of the diffuse layer has occurred because the potential has been stepped from more negative to more positive of the potential of zero charge. This is not the case when E_{pzc} has other values, but it is a general observation that the EDL becomes more

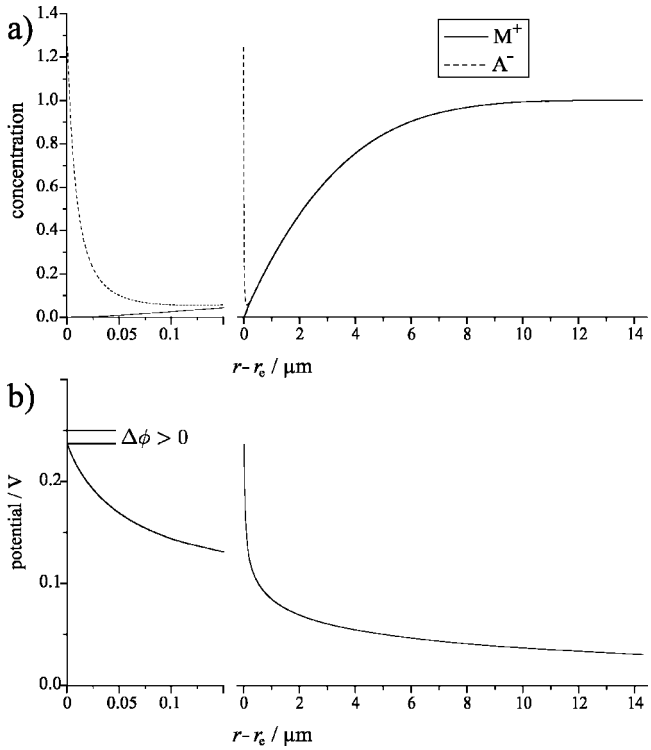

Figure 4. Profiles of (a) the dimensionless concentration and (b) the potential through solution at a 10 μm hemisphere 0.01 s after the potential step. The electroactive species is charged ($z_A = -1$), there is no additional supporting electrolyte, and $E_{pzc} = 0$ V. The region near the electrode is shown twice for greater detail.

negative or less positive in character after the potential step. The recharging of the double layer has distorted the electric field so that it is largely contained to the region close to the electrode, although there is still a significant potential gradient at larger distances, such that migration will contribute to the mass transport of the charged species. The value of $\Delta\phi$ is now positive, so there is significant oxidation of species A^- at the electrode. This has led to a depletion layer of species A extending approximately 10 μm into solution. Note that the electroinactive species M^+ has migrated away from the electrode and has a very similar concentration profile to species A^- outside of the EDL.

Figure 5 shows concentration and potential profiles for the same system after 0.01 s but at a 100 nm radius hemisphere. At this smaller electrode radius, there is less distinction between the diffuse EDL and the depletion layer. Figure 5 also shows the effect that the parameter E_{pzc} has on the structure of the electrical double layer and the solution potential at the PET. The potential driving force, $\Delta\phi$, is greatest at positive values of E_{pzc}, but the electrode surface concentration of the electroactive species A^- is greatest when E_{pzc} is negative and there must be an excess of anions in the diffuse layer. The rate of electron transfer is therefore balanced by these two competing factors. Furthermore, the potential gradient through the depletion layer favors the migration of the electroactive species toward the electrode at more negative values of E_{pzc}.

When the electroactive species is uncharged, the parameter E_{pzc} will affect the potential driving force, the surface concentration of the charged electrode product B^+, and the migration of this charged product away from the electrode. Again, the rate of electron transfer will be balanced by these competing factors

3.3. Simulated Current−Time Response. The current driven at the electrode surface is a complicated function of the surface concentrations of the reactant species, A, the product, B, and also of the potential at the PET as described by eq 14. As was shown in subsection 3.2, each of these variables has a complicated variation with time, which makes the simulated chronoamperometry correspondingly complicated to interpret. Often an observed feature of a chronoamperogram cannot be satisfactorily explained without resorting to a complete description of the concentration profiles of each species in solution. In this section, we describe some of the interesting features of the simulated current and attempt to interpret them in terms of what is likely to be the most contributing factor.

Current−time behavior is presented here as a plot of $\log_{10} i/i_{lim}$ versus $\log_{10} t$. Logarithms are used because the observed behavior spans many orders of magnitude in terms of both time and current. A fully supported diffusion-only curve will be shown in each plot for comparison. This diffusion-only line is linear with a gradient of −0.5 at short times as predicted by the Cottrell equation and flattens out to a steady-state current at long times as described by eq 21.

Figure 6 shows simulated current−time curves for various poorly supported systems at a 10 μm hemisphere. The left-hand side of the figure shows the total current including faradaic and nonfaradaic contributions while right-hand side shows the faradaic contribution only. These two sets of graphs differ considerably at times less than 10^{-4} s where the majority of the current is due to nonfaradaic contributions. At times less than approximately 10^{-5} s, the behavior of the faradaic current is highly unusual, which is attributed to the slightly delayed response of the electric field near the electrode to the change in applied potential. Starting at $t \approx 10^{-5}$ s the faradaic current increases by typically 2 or more orders of magnitude. This signficant increase is due to the potential driving force becoming more favorable for electrolysis as the more negatively charged double layer is established, as described in subsection 3.2.

At much longer times, the electron transfer is sufficiently fast that the current is limited only by mass transport of the electroactive species. In this limit, the current decreases with time, as the depletion layer expands away from the electrode. When the electroactive species is uncharged (Figure 6b) the current−time behavior in this limit is exactly that predicted by a diffusion only model. However, when the species is negatively charged (Figure 6a) there is an enhancement in current compared to the diffusion-only model at long times because migration of A^- along the positive potential gradient toward the electrode gives an additional contribution to mass transport. In all cases, the current tends toward a steady-state mass transport-limiting current, which is typical behavior for a microelectrode. It is seen from Figure 6 how the potential of zero charge influences the simulated current. This happens because it affects the makeup of the diffuse EDL, which in turn determines both the driving force of the electron transfer and the potential profile across the depletion layer.

Figure 7 shows simulated chronoamperometry at a 100 nm radius hemispherical electrode for some poorly supported systems. Typically, nonfaradaic processes dominate the measured current at short times, but then have negligible contributions after approximately 10^{-5} s. As with the 10 μm electrode, there is a rise in the faradaic current at very short times, with a maximum occurring in most cases at approximately 10^{-6} s. The mass transport limiting current is greatly influenced by the potential of zero charge, more so than was observed at the 10 μm electrode. This is because the double layer and the depletion

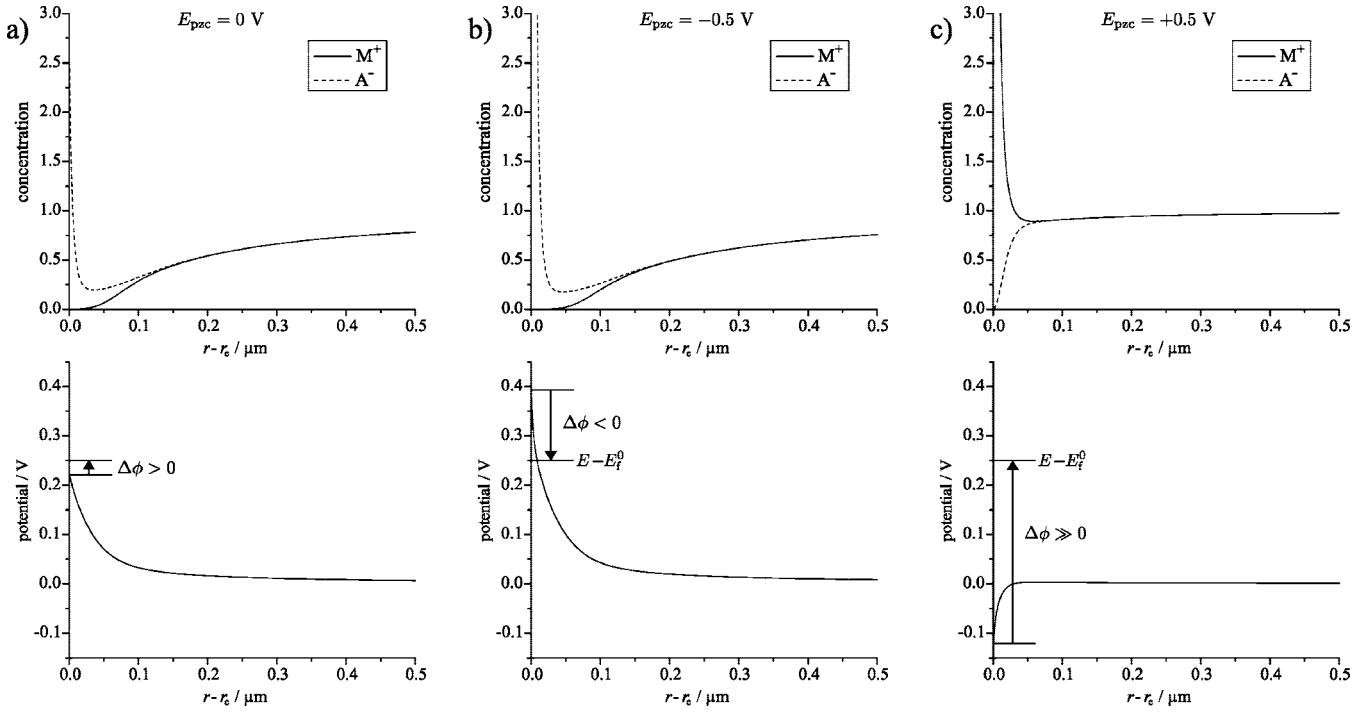

Figure 5. Simulated concentration and potential profiles at a 100 nm hemisphere 0.01 s after the potential step. The electroactive species is charged ($z_A = -1$), and there is no additional supporting electrolyte. E_{pzc} (a) 0 V, (b) −0.5 V, (c) +0.5 V.

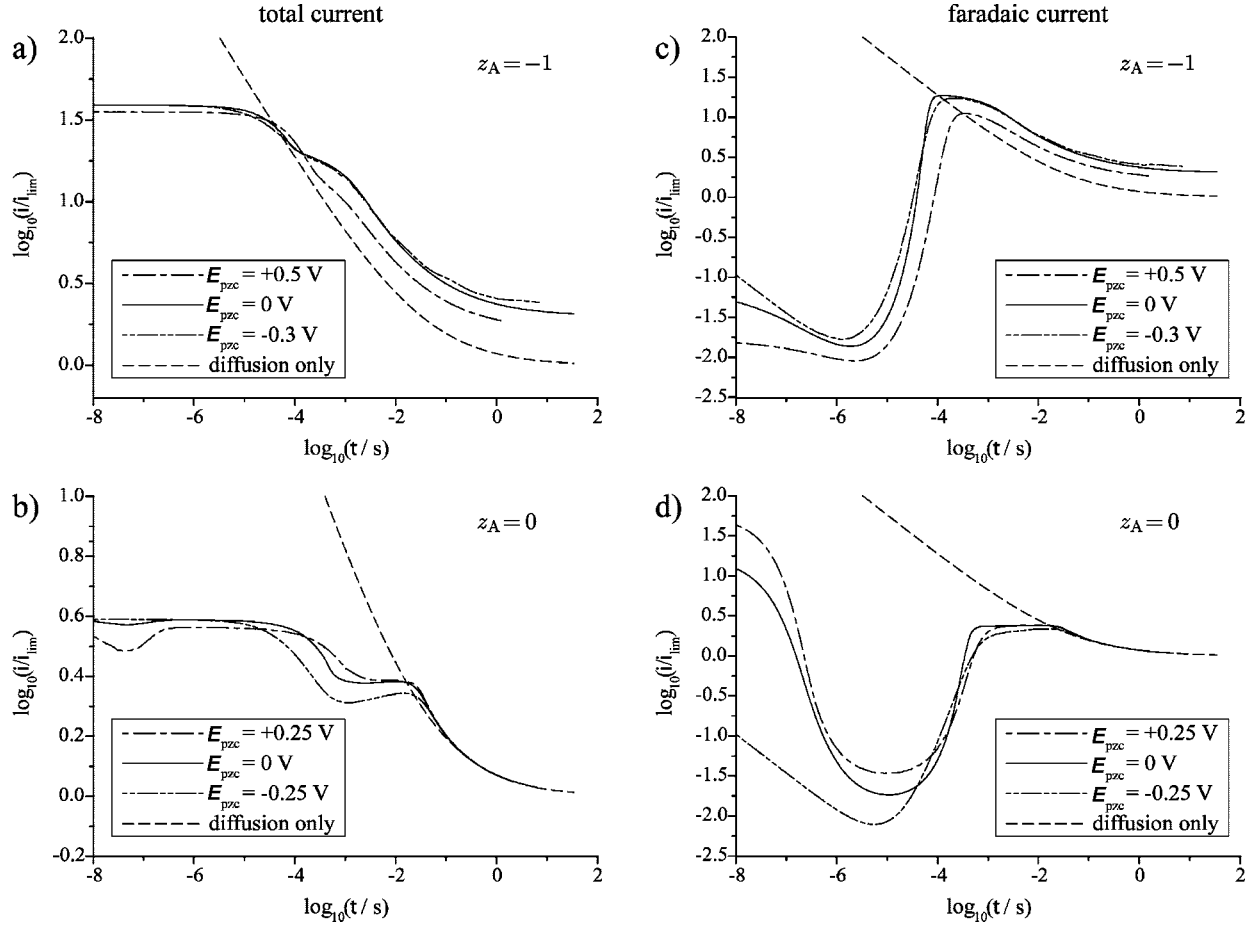

Figure 6. Simulated chronoamperometry at a 10 μm hemisphere: (a and c) charged electroactive species with no additional supporting electrolyte; (b and d) neutral electroactive species with 0.1 mM supporting electrolyte. Panels (a) and (b) show the total current; panels (c) and (d) show the faradaic contribution only.

layer are similar in size at such a small electrode, which means the makeup of the EDL has more influence on the mass transport of the electroactive species. It was described in subsection 3.2 how there are various opposing and competing factors that

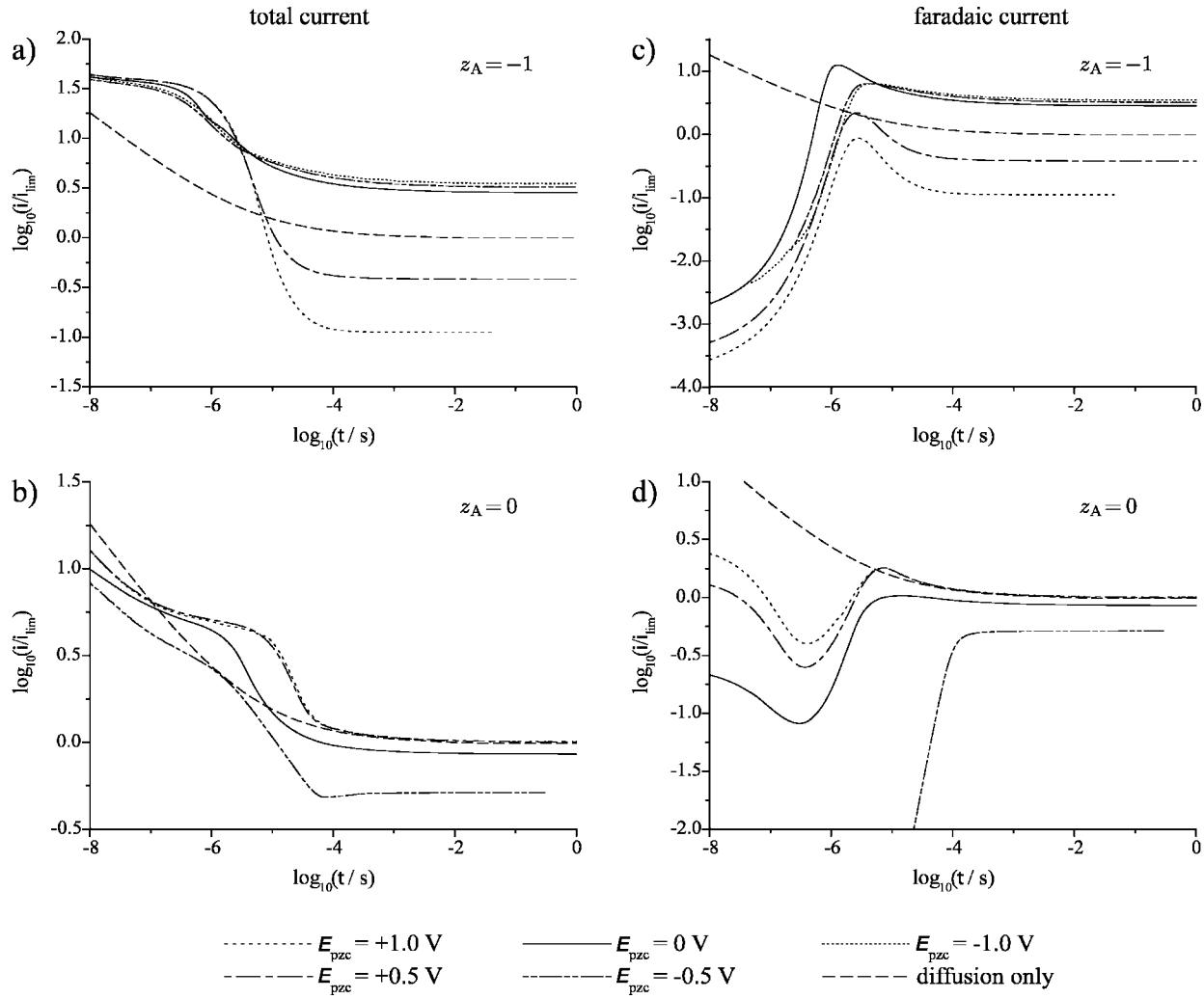

Figure 7. Simulated chronoamperometry at a 100 nm hemisphere: (a and c) charged electroactive species with no additional supporting electrolyte; (b and d) neutral electroactive species with 0.1 mM supporting electrolyte. Panels (a) and (b) show the total current; panels (c) and (d) show the faradaic contribution only.

determine the effect of the parameter E_{pzc} on the magnitude of the simulated current. It is interesting to note from Figure 7 that when the electroactive species is uncharged the smallest steady-state currents are driven with negative values of E_{pzc}, whereas the converse is seen when the electroactive species is negatively charged.

Figure 8 shows simulated chronoamperometry at a 100 nm radius electrode but this time with a large amount of supporting electrolyte ($C_{sup} = 100$). For times greater than 10^{-6} s there is excellent agreement between our model using the NPP equations and the diffusion only model; before this time the nonfaradaic contribution to the current makes the diffusion only model unsuitable. The effect of the parameter E_{pzc} on the current is greatly reduced. With such high concentrations of ions in solution, the electric field is very compact and therefore has very little effect on the mass transport of the electroactive species or on the electron transfer kinetics.

Figure 8 shows simulated chronoamperometry at a 100 nm radius electrode but this time with a large amount of supporting electrolyte ($C_{sup} = 100$). With such high concentrations of ions in solution, the electric field at the electrode is very compact and therefore has very little effect on the mass transport of the electroactive species or on the electron transfer kinetics. The current−time curve shown in Figure 8 is for a charged

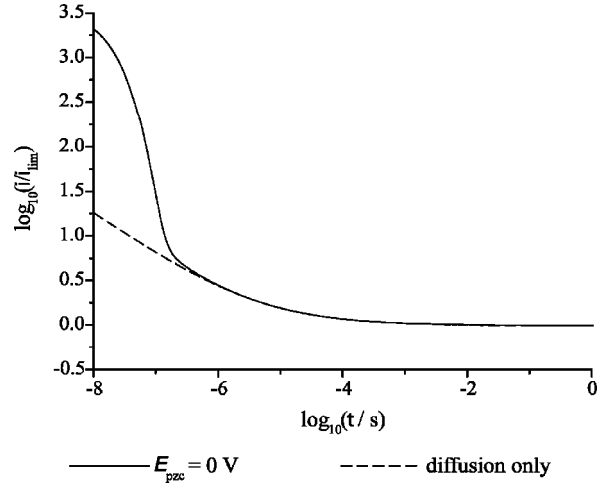

Figure 8. Simulated chronoamperometry for a charged electroactive species at a 100 nm hemisphere with 100 mM supporting electrolyte.

electroactive species with $E_{pzc} = 0$ V. Simulations using an uncharged species or with different values of E_{pzc} produced current−time curves virtually identical to the one in the Figure 8. For times greater than 10^{-6} s there is excellent agreement between our model using the NPP equations and the diffusion

only model; before this time, the nonfaradaic contribution to the current makes the diffusion-only model unsuitable.

4. Further Approximations to the Model

The numerical simulations presented in section 3 give a description of the current−time behavior expected for a faradaic process using a model that includes a detailed description of the electrical double layer. However, the model used was not necessarily the most efficient for all conditions. For example, the detailed description of the electrical double layer was probably not needed under conditions where the nature of the double layer had little effect on the current (e.g., Figure 6 at long times). The simulation grid requires a high density of mesh points in the region of the electrode to accurately model the concentration gradients in the diffuse double layer. Elimination of the EDL from the model will allow lower mesh densities to be used, therefore reducing the number of calculations to be performed by a processor in a single simulation

In this section, we present two approximations that can allow us to neglect the diffuse double layer, while potentially retaining a high degree of accuracy under some conditions.

4.1. Negligibly Small Double Layer. The simplest way to eliminate the double layer from the model is to replace the boundary condition for the potential at the PET (eq 17) with the following expression at the electrode surface:

$$\frac{\partial \theta}{\partial y} = 0 \tag{22}$$

Boundary condition (22) states that there is no electric field in solution at the electrode surface. The physical implication of this condition is that there is an infinitesimally narrow electrical double layer in which the charge in solution is equal and opposite to the charge on the surface of the electrode. The electron transfer is then driven by the potential difference between the working electrode and the point in solution immediately beyond the ideally narrow EDL. This simplifying approximation is expected to be appropriate when the depletion layer is much greater larger than the diffuse EDL. This corresponds to large microelectrodes, for example the 10 μm hemisphere featured in Figure 6.

This simple change in boundary condition has a few notable effects on the simulation procedure. The parameters E_{pzc}, μ, μ_i, ϵ_{oc}, and ϵ_{ic} are no longer necessary parameters for the simulations since they only ever appeared in boundary condition (17), which has now been replaced. This reflects how the structure of the EDL is not important when it is infinitesimally narrow. The calculated current no longer has a nonfaradaic contribution because the EDL is completely formed immediately after the potential step, and there is no subsequent charging of the electrode surface

4.2. Electroneutrality. The approximation of electroneutrality is based on the observation that there is often very little separation of positive and negative ions outside of the diffuse EDL. It was originally applied to model faradaic processes in weakly supported media because it led to analytical expressions for the steady state limiting current.[18−20] The approximation continued to be used by researchers calculating the current−time behavior of transient experiments.[23−26] The electrical double layer does not feature in this model; it is assumed that its size is significantly smaller than the depletion layer thickness. Within this model it is still possible to have a large potential drop across the depletion layer, which is entirely due to current flowing through a resistive solution, and it affects the migration of the charged species and the kinetics of the electron transfer

The electroneutrality equations were formulated in slightly different ways by the different groups of researchers. The formulation used in this section is based on Amatore's approach for a steady-state faradaic electron transfer,[19,20] but adapted to give the transient current response. The key assumption made in all the formulations is that the solution remains electrically neutral at all times and at every point in solution. This is expressed mathematically as

$$\sum_i z_i c_i = 0 \tag{23}$$

Within this approximation, the mass transport of each species is described by the Nernst−Planck expression in the form of eq 10. Amatore showed that the implication of this assumption is that the sum of the concentrations of all species at any time and location is a constant, which is denoted γ in this paper[19]

$$\sum_i c_i = \gamma \tag{24}$$

The mass transport of the electroactive species is a function of the potential profile in solution (eq 10). The flux of the electroactive species through the electrode is described by Butler−Volmer kinetics, which also depends on the potential profile (eq 14). In this model, the potential profile is simply that which can simultaneously satisfy the mass transport equations, the Butler−Volmer boundary condition and the electroneutrality condition (eq 23). Note that, in this formulation of the electroneutrality equations, the simulated potential profile does not necessarily satisfy the Poisson equation. In fact, the Poisson equation can be used to indicate the validity of the electroneutrality approximation: significant deviation from Poisson behavior suggests a more accurate model may be required. Amatore's paper derived an equation that relates the potential gradient at any point in solution to the faradaic flux through the electrode.[19] Applied to our electrochemical system, this relationship is given by eq 25 in the case when the electroactive species is charged ($z_A = -1$) or eq 26 when it is neutral ($z_A = 0$).

$$\frac{\partial \theta}{\partial y} = \frac{J_A}{\gamma - c_B} \tag{25}$$

$$\frac{\partial \theta}{\partial y} = \frac{J_A}{\gamma - c_A} \tag{26}$$

The concentration profiles of species A and B and the potential profile are found by simultaneously solving eqs 10 for both species and either eq 25 or 26 depending on the charge of species A. Boundary conditions are applied at $y = 1$ to describe the bulk concentrations of both species, and at $y = 0$ to describe the flux of the species at the electrode using Butler−Volmer kinetics as described by eq 14.

4.3. Simulated Chronoamperometry from Different Models. Figure 9 shows a comparison of the suggested models for calculating current−time curves for some electrochemical systems. The line labeled "full model" refers to the approach described in section 2, which includes a description of the EDL. The lines labeled "no EDL" and "electroneutrality" refer to the approximations described in subsections 4.1 and 4.2, respectively.

Figure 9a is for a charged electroactive species with no additional supporting electrolyte at a 10 μm radius electrode. Both the approximations show qualitatively good agreement with the full model at long times where the depletion layer is large compared to the electrical double layer. At short times, there is poor agreement, since the structure of the EDL has a

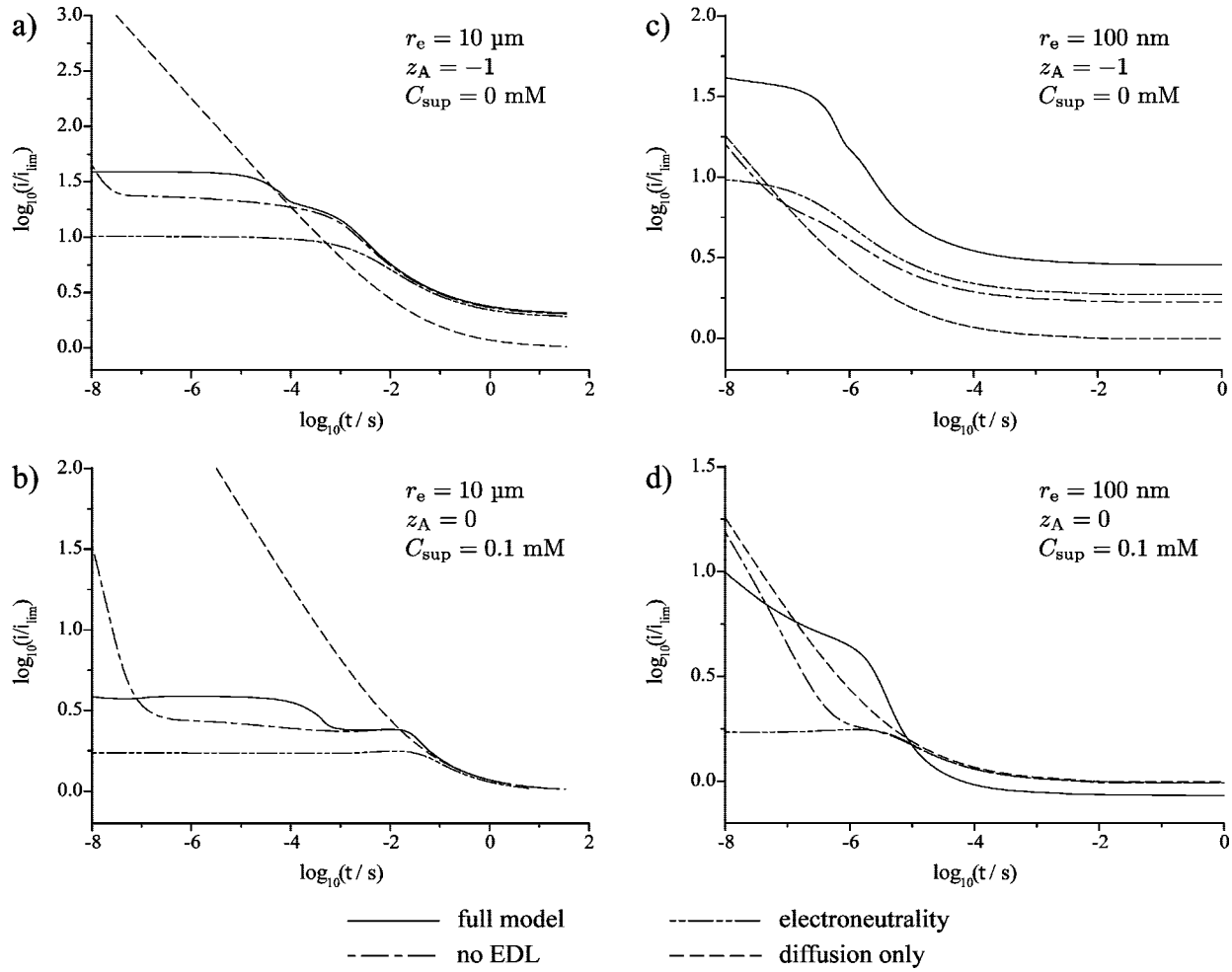

Figure 9. Comparison of various models for simulating chronoamperometry of various systems as described in the figures. $E_{pzc} = 0$ V. Parts a−d are for differently charged electroactive species and differently sized electrodes as described in the figure.

greater influence on mass transport and electrode kinetics. The approximation of a negligibly small double layer is successful at times greater than $t \approx 10^{-4}$ s, and the approximation of electroneutrality is successful at times greater than $t \approx 0.01$ s. Figure 9b is for a neutral electroactive species in poorly supported solution, also at a 10 μm radius electrode. For this system, the approximation of a negligibly small double layer is successful at times greater than $t \approx 10^{-3}$ s. The electroneutrality approximation agrees with the full model at times greater than $t \approx 0.07$ s; however, it is interesting that this approximation is no more successful than simple diffusion-only model, which also agrees with the full model over the same time period. It should be noted that we have only made comparisons with the full model using $E_{pzc} = 0$ V. However, it was shown in subsection 3.3 that at a 10 μm electrode the parameter E_{pzc} has only a small influence on the simulated currents at the times for which the approximations have been described as successful.

Parts c and d of Figure 9 are for the same electrochemical systems but at a 100 nm radius electrode. At this small radius the diffuse part of the EDL is large compared to the depletion layer and therefore has a significant influence on mass transport of the electroactive species and on the kinetics of the electron transfer. It is therefore no surprise that neither of the approximations shows agreement with the time−current curves predicted by the full model.

5. Conclusions

Electrochemical experiments in solutions of low ionic strength can be treated theoretically using the model described in section 2. Concentration profiles, potential profiles, and current−time curves have been presented here for a potential step chronoamperometry experiment, giving an insight into the predicted effects of using low amounts of supporting electrolyte. Despite using a fairly simple description of the EDL, this work demonstrates the magnitude of the influence that the structure of the electrode−solution interface has on the faradaic current. The model used could also be applied to model other transient electrochemical experiments, for example potential sweeps.

The continued success of any model depends on the ease with which it can be applied to real experimental systems of interest. It is in this respect that the model described in section 2 shows two weaknesses. First of all, it requires values for a large number of physical parameters of the system, some of which are not easily measurable. Second, the calculations are computationally expensive and CPU simulation times are long. This is partly because of the slow iterative process required to solve the nonlinear NPP equations. A large number of time steps are required, as the iterative process often fails to converge on an answer if the value $\Delta\tau$ is too large. Furthermore, the simulation grid requires a high density of nodes in the region of the diffuse double layer.

The complexity of the theoretical model is illustrated by considering how many physical parameters are needed to calculate the current in the potential step experiment. In a diffusion-only system, the current measured depends only on the diffusion coefficient and concentration of the electroactive species, and the radius of the electrode. At short times where

the measured current may be limited by the rate of electron transfer, the following parameters are also important: the heterogeneous rate constant, the charge transfer coefficient, the electrode potential, and the formal electrode potential. The model used in this paper for poorly supported chronoamperometry requires values for all the parameters already mentioned. It also requires values for the concentration of each charged species present in solution, the dielectric constant of bulk solution, the dimensions and the dielectric constants of the compact part of the EDL, the electrode potential of zero charge, and the electrode potential immediately before the potential step. For many experimental systems the exact details of the compact double layer and the potential of zero charge will not be known.

Given the complexity of the full model and the long simulations times associated with it, there is a lot of appeal in using one of the approximations described in section 4. In fact, to the best of our knowledge, all other theoretical treatments of poorly supported transient chronoamperometry have made use of the electroneutrality approximation. The work presented in this paper has allowed for the first time a comparison of the electroneutrality approximation with a more complete model. Calculations using the approximations described in section 4 have shorter CPU simulation times, because fewer nodes are required in the region near the electrode, the iterative process is stable for larger values of $\Delta\tau$, and often fewer iterations of the Newton−Raphson method are needed before it converges on a stable concentration profile. We found that the approximation of a negligibly small double layer led to the shortest simulation times, with the approximation of electroneutrality in second place.

The approximations in section 4 are only appropriate when the depletion layer at the electrode is greater than the diffuse part of the electrical double layer. This corresponds to larger microelectrodes and only at longer times. When the approximations were successful, it was generally found that the approximation of a negligibly small double layer agreed with the full model at shorter times than did the approximation of electroneutrality

For modeling poorly supported electrochemical experiments at sufficiently large electrodes, we recommend using the approximation of a negligibly small double layer as described in subsection 4.1. This model appears to be more accurate than the model of electroneutrality, it is no more difficult to implement, and the equations are typically solved with much shorter CPU simulation times.

Acknowledgment. I.S. thanks the Engineering and Physical Sciences Research Council for financial support.

Appendix 1: Derivation of Equation 17

The boundary condition that describes the potential at the PET is found by consideration of the electric field across the compact double layer. The Poisson equation is applied using the transformed coordinate y to give the following expression which is valid across the entire electroneutral region:

$$\frac{\partial^2(\epsilon_r\theta)}{\partial y^2} = 0 \tag{27}$$

Equation 27 implies that the potential gradient $\partial\theta/\partial y$ is uniform throughout the inner part and then uniform throughout the outer part of the compact EDL, noting that these two regions have different local dielectric constants. The potential profile across the compact double layer is shown in Figure 10. Equation 27 further implies that the potential gradients in each region are related by the local dielectric constants

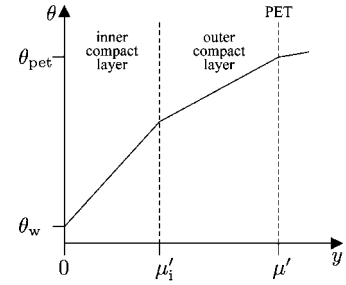

Figure 10. Potential profile across the compact double layer in terms of the y-coordinate system.

$$\epsilon_s\left(\frac{\partial\theta}{\partial y}\right)_{pet} = \epsilon_{ic}\left(\frac{\partial\theta}{\partial y}\right)_{ic} = \epsilon_{oc}\left(\frac{\partial\theta}{\partial y}\right)_{oc} \tag{28}$$

where the label pet refers to the potential gradient at the PET but in the diffuse part of the double layer, and the labels ic and oc refer to the inner and outer compact layers, respectively.

A geometric assessment of Figure 10 leads to an expression for θ_{pet} as the sum of potential terms

$$\theta_{pet} = \theta_w + \mu'_i\left(\frac{\partial\theta}{\partial y}\right)_{ic} + (\mu' - \mu'_i)\left(\frac{\partial\theta}{\partial y}\right)_{oc} \tag{29}$$

Equation 17 is then found by substituting the expressions in eq 28 into eq 29. For convenience, the dimensionless parameters μ' and μ'_i are rewritten in terms of their dimensional counterparts. It has also been noted that in our model where the potential is defined relative to the bulk solution potential, $\theta_s = 0$, the working electrode potential can be expressed in terms of the known potential differences E and E_{pzc}

$$\theta_w = \frac{F}{RT}(E - E_{pzc}) \tag{30}$$

An alternative derivation of eq 17 involves applying Gauss's law to describe the electric field in the compact layer in terms of the charge residing on the electrode surface. This alternative derivation was presented in the paper of He et al.[12]

Appendix 2: Numerical Methods

Newton−Raphson Method

The nonlinear system of NPP equations described in subsection is solved using the matrix form of the Newton−Raphson method. In this method, a vector $\mathbf{x}$ contains all the unknown variables to be found, labeled x_0, x_1,..., x_n. The system of equations to be solved is in the form $\mathbf{F}(\mathbf{x}) = 0$, where the vector $\mathbf{F}(\mathbf{x})$ contains the equations $f_0(\mathbf{x})$, $f_1(\mathbf{x})$,..., $f_n(\mathbf{x})$. A vector $\mathbf{u}$ is introduced where $\mathbf{u} = \mathbf{u}^{z+1} - \mathbf{u}^z$, which represents the difference between successive iterations of Newton's method. The iterative formula is then given by

$$\mathbf{Ju} = -\mathbf{F} \tag{31}$$

where $\mathbf{J}$ is the matrix in eq 32. The procedure is iterated until the termination criterion $|x^{z+1} - x^z| < \epsilon$ is met for all unknowns, where ϵ is chosen to be a suitably small number

NPP Equations

The NPP equations described in subsection 2.2 are discretized over an expanding grid containing n grid points. The vectors $\mathbf{x}$ and $\mathbf{F}$ for the nonlinear NPP equations are given by eq 33, where the label j refers to the point on the spatial grid, and the label $k + 1$ indicates that the unknowns are for the next time step

$$\mathbf{J} = \begin{bmatrix} \frac{\partial f_0}{\partial x_0} & \frac{\partial f_0}{\partial x_1} & \cdots & \frac{\partial f_0}{\partial x_n} \\ \frac{\partial f_1}{\partial x_0} & \frac{\partial f_1}{\partial x_1} & \cdots & \frac{\partial f_1}{\partial x_n} \\ \vdots & \vdots & \ddots & \vdots \\ \frac{\partial f_n}{\partial x_0} & \frac{\partial f_n}{\partial x_1} & \cdots & \frac{\partial f_n}{\partial x_n} \end{bmatrix} \tag{32}$$

$$\mathbf{x} = \begin{bmatrix} c_{\mathrm{A},0}^{k+1} \\ c_{\mathrm{B},0}^{k+1} \\ \theta_0^{k+1} \\ c_{\mathrm{M}^+,0}^{k+1} \\ c_{\mathrm{X}^-,0}^{k+1} \\ \vdots \\ c_{\mathrm{A},j}^{k+1} \\ c_{\mathrm{B},j}^{k+1} \\ \theta_j^{k+1} \\ c_{\mathrm{M}^+,j}^{k+1} \\ c_{\mathrm{X}^-,j}^{k+1} \\ \vdots \\ c_{\mathrm{A},n}^{k+1} \\ c_{\mathrm{B},n}^{k+1} \\ \theta_n^{k+1} \\ c_{\mathrm{M}^+,n}^{k+1} \\ c_{\mathrm{X}^-,n}^{k+1} \end{bmatrix} \quad \mathbf{F} = \begin{bmatrix} f_{\mathrm{A},0}(\mathbf{x}) \\ f_{\mathrm{B},0}(\mathbf{x}) \\ f_{\theta,0}(\mathbf{x}) \\ f_{\mathrm{M}^+,0}(\mathbf{x}) \\ f_{\mathrm{X}^-,0}(\mathbf{x}) \\ \vdots \\ f_{\mathrm{A},j}(\mathbf{x}) \\ f_{\mathrm{B},j}(\mathbf{x}) \\ f_{\theta,j}(\mathbf{x}) \\ f_{\mathrm{M}^+,j}(\mathbf{x}) \\ f_{\mathrm{X}^-,j}(\mathbf{x}) \\ \vdots \\ f_{\mathrm{A},n}(\mathbf{x}) \\ f_{\mathrm{B},n}(\mathbf{x}) \\ f_{\theta,n}(\mathbf{x}) \\ f_{\mathrm{M}^+,n}(\mathbf{x}) \\ f_{\mathrm{X}^-,n}(\mathbf{x}) \end{bmatrix} \tag{33}$$

The equations $f_{\mathrm{A},j}, f_{\mathrm{B},j}, f_{\mathrm{M}^+,j}$ and $f_{\mathrm{X}^-,j}$, are the discretized mass transport equations for $0 < j < n$. For example, $f_{\mathrm{M}^+,j}(\mathbf{x})$ is the discretized version of the following equation

$$-\frac{\partial c_{\mathrm{M}^+}}{\partial \tau} + \frac{(1-y)^4}{{R_\mathrm{e}}^2}\left(\frac{\partial^2 c_{\mathrm{M}^+}}{\partial y^2} + c_{\mathrm{M}^+}\frac{\partial^2 \theta}{\partial y^2} + c_{\mathrm{M}^+}\frac{\partial c_{\mathrm{M}^+}}{\partial y}\frac{\partial \theta}{\partial y}\right) = 0 \tag{34}$$

The equation $f_{\theta,j}(x)$ is the discretized version of the following form of the Poisson equation:

$$\frac{(1-y)^4}{{R_\mathrm{e}}^2}\frac{\partial^2 \theta}{\partial y^2} + c_{\mathrm{M}^+} - c_{\mathrm{X}^-} + z c_\mathrm{A} + (z+1)c_\mathrm{B} = 0 \tag{35}$$

The following discretizations are used:

$$\frac{\partial c}{\partial \tau} \approx \frac{c_j^{k+1} - c_j^k}{\Delta \tau} \tag{36}$$

$$\frac{\partial^2 c}{\partial y^2} \approx \frac{c_{j+1} - c_j}{0.5\Delta^+ y(\Delta^+ y + \Delta^- y)} - \frac{c_j - c_{j-1}}{0.5\Delta^- y(\Delta^+ y + \Delta^- y)} \tag{37}$$

$$\frac{\partial^2 \theta}{\partial y^2} \approx \frac{\theta_{j+1} - \theta_j}{0.5\Delta^+ y(\Delta^+ y + \Delta^- y)} - \frac{\theta_j - \theta_{j-1}}{0.5\Delta^- y(\Delta^+ y + \Delta^- y)} \tag{38}$$

$$\frac{\partial \theta}{\partial y} \approx \frac{\theta_{j+1} - \theta_{j-1}}{\Delta^+ y + \Delta^- y} \tag{39}$$

where $\Delta^+ y$ refers to the spacing between grid points j and $j+1$, and $\Delta^- y$ refers to the spacing between grid points j and $j-1$. The labels k and $k+1$ have been removed from eqs 37, 38, and 39 for clarity. The Crank−Nicolson discretization of time is used, which is expected to be more accurate than a fully implicit scheme.[37]

The equations $f_{\mathrm{A},0}, f_{\mathrm{B},0}, f_{\theta,0}, f_{\mathrm{M}^+,0}$, and $f_{\mathrm{X}^-,0}$ are the discretized forms of the boundary conditions at the electrode surface given in Table 1. For example

$$f_{\mathrm{M}^+,0}(\mathbf{x}) = \frac{c_{\mathrm{M}^+,1} - c_{\mathrm{M}^+,0}}{\Delta y} + c_{\mathrm{M}^+,0}\frac{\theta_1 - \theta_0}{\Delta y} = 0 \tag{40}$$

The equations $f_{\mathrm{A},n}, f_{\mathrm{B},n}, f_{\theta,n}, f_{M^+,n}$, and $f_{\mathrm{X}^-,n}$ are the boundary conditions at $y = 1$ given in Table 1. For example

$$f_{\mathrm{M}^+,n}(\mathbf{x}) = c_{\mathrm{M}^+,n} - c_\mathrm{sup} = 0 \tag{41}$$

The matrix $\mathbf{J}$ is found by differentiating equations $\mathbf{F}(\mathbf{x})$ as described in eq 32. Matrix $\mathbf{J}$ has nonzero elements only on its central 15 diagonal lines. The matrix eq 31 can therefore be solved using a generalized form of the Thomas algorithm.

$$\mathbf{x} = \begin{bmatrix} c_{\mathrm{A},0}^{k+1} \\ \theta_0^{k+1} \\ c_{\mathrm{B},0}^{k+1} \\ J_{\mathrm{e},0}^{k+1} \\ \vdots \\ c_{\mathrm{A},j}^{k+1} \\ \theta_j^{k+1} \\ c_{\mathrm{B},j}^{k+1} \\ J_{\mathrm{c},j}^{k+1} \\ \vdots \\ c_{\mathrm{A},n}^{k+1} \\ \theta_n^{k+1} \\ c_{\mathrm{B},n}^{k+1} \\ J_{\mathrm{c},n}^{k+1} \end{bmatrix} \quad \mathbf{F} = \begin{bmatrix} f_{\mathrm{A},0}(\mathbf{x}) \\ f_{\theta,0}(\mathbf{x}) \\ f_{\mathrm{B},0}(\mathbf{x}) \\ f_{J,0}(\mathbf{x}) \\ \vdots \\ f_{\mathrm{A},j}(\mathbf{x}) \\ f_{\theta,j}(\mathbf{x}) \\ f_{\mathrm{B},j}(\mathbf{x}) \\ f_{J,j}(\mathbf{x}) \\ \vdots \\ f_{\mathrm{A},n}(\mathbf{x}) \\ f_{\theta,n}(\mathbf{x}) \\ f_{\mathrm{B},n}(\mathbf{x}) \\ f_{J,n}(\mathbf{x}) \end{bmatrix} \tag{42}$$

Electroneutrality Equations

The electroneutrality equations are discretized over an expanding grid containing n grid points. The vectors $\mathbf{x}$ and $\mathbf{F}$ for these equations are given by eq 42, where the labels j and k have the same meaning as in eq 33. The concentrations of the inert species c_{M^+} and c_{X^-} do not appear in x, but they can be inferred from eqs 23 and 24.

The value J_e represents the faradaic flux of the electroactive species through the electrode, and therefore should only have a single value, despite appearing in the vector $\mathbf{x}$ a number of times. The equation $f_{J,j}$ for $j > 0$ is therefore

$$f_{J,j} = J_{e,j-1} - J_{e,j} = 0 \tag{43}$$

The quantity J_e is deliberately made to appear in the vector $\mathbf{x}$ a large number of times because it will lead to a matrix $\mathbf{J}$ which will be diagonally dominant. The equations $f_{A,j}$ and $f_{B,j}$ for $0 < j < n$ are discretised versions the mass transport equations, as described in the previous section. The equation $f_{\theta,j}$ for $0 \leq j < n$ is the discretized version of eq 25 when the electroactive species is charged, or eq 26 when it is neutral. The equations $f_{A,0}$, $f_{B,0}$, $f_{A,n}$, $f_{B,n}$, and $f_{\theta,n}$ are the boundary conditions as described in the previous section.

Matrix $\mathbf{J}$ for this system of equations has nonzero elements only on its central 11 diagonal lines. The matrix eq 31 is therefore solved using a generalized form of the Thomas algorithm.

Equilibrium Double Layer

The equilibrium double layer is found by first solving eq 19 for the equilibrium potential profile. The equation is discretized over an expanding spatial grid. The vectors $\mathbf{x}$ and $\mathbf{F}$ are given by

$$\mathbf{x} = \begin{bmatrix} \theta_0 \\ \theta_1 \\ \vdots \\ \theta_j \\ \vdots \\ \theta_n \end{bmatrix} \quad \mathbf{F} = \begin{bmatrix} f_{\theta,0}(\mathbf{x}) \\ f_{\theta,1}(\mathbf{x}) \\ \vdots \\ f_{\theta,j}(\mathbf{x}) \\ \vdots \\ f_{\theta,n}(\mathbf{x}) \end{bmatrix} \tag{44}$$

where $f_{\theta,j}(\mathbf{x})$ is the discretized form of eq 19 for $0 < j < n$. The equation $f_{\theta,0}(\mathbf{x})$ is the boundary condition in eq 17, and the equation $f_{\theta,n}(\mathbf{x})$ is the boundary condition setting $\theta = 0$ at $y = 1$. Matrix $\mathbf{J}$ has nonzero elements only on its central three diagonal lines, so the matrix eq 31 is solved using the Thomas algorithm.

References and Notes

(1) Cottrell, F. G. *Z. Phys. Chem.* **1903**, *42*, 385–431.
(2) Bond, A. M.; Fleischmann, M.; Robinson, J. *J. Electroanal. Chem.* **1984**, *168*, 299–312.
(3) Cassidy, J.; Khoo, S. B.; Pons, S.; Fleischmann, M. *J. Phys. Chem.* **1985**, *89*, 3933–3935.
(4) Bond, A. M.; Lay, P. A. *J. Electroanal. Chem.* **1986**, *199*, 285–295.
(5) Albery, W. J. *Electrode Kinetics*; Clarendon Press: Oxford, UK, 1975.
(6) Buck, R. P. *J. Electroanal. Chem. Interfacial Electrochem.* **1973**, *46*, 1–23.
(7) Norton, J. D.; White, H. S.; Feldberg, S. W. *J. Phys. Chem.* **1990**, *94*, 6772–6780.
(8) Murphy, W. D.; Manzanares, J. A.; Mafé, S.; Reiss, H. *J. Phys. Chem.* **1992**, *96*, 9983–9991.
(9) Smith, C. P.; White, H. S. *Anal. Chem.* **1993**, *65*, 3343–3353.
(10) Oldham, K. B.; Bond, A. M. *J. Electroanal. Chem.* **2001**, *508*, 28–40.
(11) Bonnefont, A.; Argoul, F.; Bazant, M. Z. *J. Electroanal. Chem.* **2001**, *500*, 52–61.
(12) He, R.; Chen, S.; Yang, F.; Wu, B. *J. Phys. Chem. B* **2006**, *110*, 3262–3270.
(13) Yang, X.; Zhang, G. *Nanotechnology* **2007**, *18*, 335201.
(14) Planck, M. *Ann. Phys. Chem.* **1890**, *39*, 161.
(15) Planck, M. *Ann. Phys. Chem.* **1890**, *40*, 561.
(16) MacInnes, D. A. *The Principles of Electrochemistry*; Dover: New York, 1961.
(17) Levich, V. G. *Physicochemical Hydrodynamics*; Prentice-Hall: Englewood Cliffs, NJ, 1962.
(18) Bond, A. M.; Fleischmann, M.; Robinson, J. *J. Electroanal. Chem.* **1984**, *172*, 11–25.
(19) Amatore, C.; Deakin, M. R.; Wightman, R. M. *J. Electroanal. Chem.* **1987**, *220*, 49–63.
(20) Amatore, C.; Fosset, B.; Bartelt, J.; Deakin, M. R.; Wightman, R. M. *J. Electroanal. Chem.* **1988**, *256*, 255–268.
(21) Oldham, K. B. *Anal. Chem.* **1997**, *69*, 446–453.
(22) Klymenko, O. V.; Amatore, C.; Svir, I. *Anal. Chem.* **2007**, *79*, 6341–6347.
(23) Jaworski, A.; Donten, M.; Stojek, Z. *Anal. Chim. Acta* **1995**, *305*, 106–113.
(24) Hyk, W.; Palys, M.; Stojek, Z. *J. Electroanal. Chem.* **1996**, *415*, 13–22.
(25) Hyk, W.; Stojek, Z. *J. Electroanal. Chem.* **1997**, *439*, 81–88.
(26) Ciszkowska, M.; Jaworski, A.; Osteryoung, J. *J. Electroanal. Chem.* **1997**, *423*, 95–101.
(27) Martuzans, B.; Skryl, Y. *J. Chem. Soc., Faraday Trans.* **1998**, *94*, 2411–2416.
(28) Sokalski, T.; Lewenstam, A. *Electrochem. Commun.* **2001**, *3*, 107–112.
(29) Sokalski, T.; Lingenfelter, P.; Lewenstam, A. *J. Phys. Chem. B* **2003**, *107*, 2443–2452.
(30) Lingenfelter, P.; Bedlechowicz-Sliwakowska, I.; Sokalski, T.; Maj-Zurawska, M.; Lewenstam, A. *Anal. Chem.* **2006**, *78*, 6783–6791.
(31) Riveros, O. J.; Croxton, T. L.; Armstrong, W. M. *J. Theor. Biol.* **1989**, *140*, 221–230.
(32) Hafemann, D. R. *J. Phys. Chem.* **1965**, *69*, 4226–4231.
(33) Brumleve, T. R.; Buck, R. P. *J. Electroanal. Chem.* **1978**, *90*, 1–31.
(34) Newman, J. *J. Phys. Chem.* **1969**, *75*, 1843–1848.
(35) Bazant, M. Z.; Thornton, K.; Ajdari, A. *Phys. Rev. E* **2004**, *70*, 021506.
(36) Bockris, J. O.; Reddy, A. K. N. *Modern Electrochemistry*; Plenum: New York, 1970.
(37) Störzbach, M.; Heinze, J. *J. Electroanal. Chem.* **1993**, *346*, 1–27.

JP804442M